Idealized Offshore Low-Level Jets for Turbine Structural Impact Considerations

Emily de Jong[1], Eliot Quon[2], and Daniel Zalkind[2]

[1]California Institute of Technology
[2]National Renewable Energy Laboratory

January 30, 2024

Abstract

Low level jets (LLJs) describe conditions in which the wind speed reaches a local maximum with respect to altitude near the surface, and have been observed intermittently in the US Mid-Atlantic offshore environment. LLJs pose unique operating conditions for future wind turbines operating in the region, presenting negative shear and locally strong veer, but they are not typically considered in existing turbine standards. This work builds upon recent research that explains the formation and evolution of U.S. Mid-Atlantic LLJs through a simple analytical governing equation. We generate several LLJ inflow conditions with varying jet characteristics based on this analytical model and create monotonically-sheared (MS) analogues with constant veer in order to assess the impacts of the LLJ on turbine performance and loading. Using aeroelastic simulations with these inflow conditions on the IEA 15MW reference turbine, we find that the LLJ leads to a greater range of tower top pitching and yawing moments, which could contribute to larger accumulated structural fatigue in components compared to monotonically-sheared inflow. These preliminary results demonstrate a path toward a unified set of test cases for low-level wind maxima that can inform International Electrotechnical Commission standards related to offshore wind turbine design.

Idealized Offshore Low-Level Jets for Turbine Structural Impact Considerations

October 29, 2023

Emily de Jong[1,*], Eliot Quon[2], Daniel Zalkind[2]
[1]California Institute of Technology, Pasadena, CA, USA
[2]National Renewable Energy Lab, Golden, CO, USA
[*]Corresponding author email: edejong@caltech.edu

Keywords: Low-level jet, aerodynamic load, FAST

Abstract

Low level jets (LLJs) describe conditions in which the wind speed reaches a local maximum with respect to altitude near the surface, and have been observed intermittently in the US Mid-Atlantic offshore environment. LLJs pose unique operating conditions for future wind turbines operating in the region, presenting negative shear and locally strong veer, but they are not typically considered in existing turbine standards. This work builds upon recent research that explains the formation and evolution of U.S. Mid-Atlantic LLJs through a simple analytical governing equation. We generate several LLJ inflow conditions with varying jet characteristics based on this analytical model and create monotonically-sheared (MS) analogues with constant veer in order to assess the impacts of the LLJ on turbine performance and loading. Using aeroelastic simulations with these inflow conditions on the IEA 15MW reference turbine, we find that the LLJ leads to a greater range of tower top pitching and yawing moments, which could contribute to larger accumulated structural fatigue in components compared to monotonically-sheared inflow. These preliminary results demonstrate a path toward a unified set of test cases for low-level wind maxima that can inform International Electrotechnical Commission standards related to offshore wind turbine design.

Acknowledgements: *E. de Jong acknowledges funding support from the U.S. Department of Energy Computational Sciences Graduate Fellowship. This material is based upon work supported by the U.S. Department of Energy's*

Office of Energy Efficiency and Renewable Energy (EERE) under the Wind Energy Technologies Office Award Number DE-EE0008390 to the New York State Energy Research and Development Authority for establishing the National Offshore Wind Research Consortium. This work was authored in part by the National Renewable Energy Laboratory, operated by Alliance for Sustainable Energy, LLC, for the U.S. Department of Energy (DOE) under contract no. DE-AC36-08GO28308.

1 Introduction

A low-level jet (LLJ) is a local maximum in the wind speed that occurs within the boundary layer, presenting a region of negative shear above this maximum or "jet nose". LLJs are typically associated with stable boundary layers and frequently exhibit much higher veer, positive or negative shear, and lower turbulence intensity than standard neutral or unstable atmospheric conditions. In the context of wind energy, LLJs have been found to produce higher aerodynamic loads [1] as well as higher power production [2], but have not been heavily studied as LLJs on land such as the nocturnal jets in the Southern Great Plains typically exhibit their maximum wind speeds above 300 m altitude [3]. However, recent studies of offshore lease areas in the U.S. Mid-Atlantic region indicate that LLJs occur intermittently at altitudes relevant to an offshore turbine as often as 7% of the time [4]. Current International Electrotechnical Commission (IEC) standards do not account for extreme shear conditions such as the low-level jet, which hinders the ability of wind turbine designers to understand and plan for the impacts of these winds. A likely reason for this exclusion is that the impacts and important features of LLJs on turbine performance and loading have not been fully quantified.

A few recent works have characterized the impacts of LLJs on turbine performance and fatigue using idealized and steady-state inflow conditions. However, a lack of standardization in the type of inflow conditions used in these studies as well as differences in the research methods used (experimental and computational) have led to conflicting results on whether LLJ conditions are expected to have a detrimental impact on turbine structures. For instance, Gutierrez et al. analyzed structural impacts of LLJs on a reference turbine using the OpenFAST multiphysics simulation tool, observing cyclical aerodynamic loads from the strong wind shear [5], reduced forces and moments [2], and propagation of characteristic LLJ frequencies to structural components of the turbine [6]. Doosttalab et al. studied these impacts and farm-scale wake effects experimentally in a wind tunnel, showing that the presence of an LLJ increased energy recovery in downstream turbines as long as the jet nose height did not coincide with the turbine hub height. Other recent studies have employed large eddy simulations (LES) to reveal the impact of the jet nose height on turbine performance [8] and wake recovery [9], with the latter study indicating as much as a 30% increase in damage equivalent loads (DEL) resulting from a LLJ compared with a typical monotonically-sheared (MS) wind profile. This work aims to present a more rigorous approach to generating LLJ inflow conditions and comparable MS conditions in order to isolate performance and structural impacts in future turbine design.

This study builds on a recent mechanistic study of the atmospheric dynamics that lead to LLJ formation in the New York (NY) Bight [10]. This previous work identified predominantly springtime LLJs from floating lidar buoy data [11], identifying a set of equations to describe the evolution of these jets that couples inertial oscillation (the Blackadar mechanism [12, 13]) and thermal wind balance induced by horizontal pressure gradients [14, 15]. In the way that a power law can be used to prescribe a monotonically increasing wind speed profile under a range of shear conditions, these LLJ equations can define a range of representative LLJ inflow conditions for numerical simulation of test turbines. This work proposes several such test cases, based on the case studies identified in [10], and presents a preliminary analysis of structural impacts on the IEA 15-MW reference wind turbine [16].

The structure of the rest of this paper is as follows: Section 2 presents the equations and properties of several idealized LLJs and their monotonically-sheared analogues; Section 3 describes the methods used to simulate and analyze turbine performance; Section 4 presents and discusses the results of this preliminary structural analysis; and Section 5 summarizes our findings, offering insights for future work.

2 Inflow Conditions

2.1 Analytical LLJ model

deJong, Quon, and Yellapantula demonstrated that for three characteristic persistent LLJs identified in the NY Bight, the evolution of the wind speed and direction could be described as an inertial rotation of the wind vector about a thermal wind balance. These equations are decomposed into a steady-state component (u_{ss}, v_{ss}) and a time-varying rotation as:

$$\begin{aligned} u(z,t) &= u_{ss}(z) + A(z)\sin(ft + \phi(z)) \\ v(z,t) &= v_{ss}(z) + A(z)\cos(ft + \phi(z)) \end{aligned} \tag{1}$$

where (u, v) are the altitude (z) dependent zonal and meridional winds, $A(z)$ is the amplitude of inertial oscillation (IO), f is the Coriolis frequency, and ϕ is the phase-shift. The height-dependence of the steady-state wind vector is further prescribed by a thermal-wind balance as an Ekman layer:

$$\begin{aligned} u_{ss}(z) &= \left(u_{g0} + u_{gz}z\right) + e^{-\eta}\Big((u_0 - u_{g0})\cos\eta + (v_0 - v_{g0})\sin\eta\Big) \\ v_{ss}(z) &= \left(v_{g0} + v_{gz}z\right) + e^{-\eta}\Big((v_0 - v_{g0})\cos\eta - (u_0 - u_{g0})\sin\eta\Big), \end{aligned} \tag{2}$$

with the surface geostrophic wind (u_{g0}, v_{g0}) matched to a surface layer

$$\frac{\partial(u_g, v_g)}{\partial z}\Big|_{z=0} = \frac{A}{H}(u_g(0), v_g(0)). \tag{3}$$

In equation 2, $\eta = z/H$ and vertical gradients in the geostrophic wind (u_{gz}, v_{gz}) are proportional to horizontal gradients in temperature via thermal wind balance. These parameters drive the wind profile in the mean state based on synoptic scale conditions such as pressure systems or fronts. The Taylor matching condition for the surface layer (3) uses the same scale height H as the Ekman layer, which is an indication of the height and therefore stability of the boundary layer. The final parameter A is a dimensionless quantity corresponding to atmospheric stability [15].

In deJong, Quon, and Yellapantula, the profiles of $A(z)$, $\phi(z)$, and $(u_{ss}(z), v_{ss}(z))$ were fit to the observational floating lidar measurements for three separate 18-hr periods from NYSERDA buoy E06 on 5 April 2020, 15 May 2020, and 3 June 2020. From the steady-state velocities from this fit, a second regression was performed to fix the six remaining parameters: $A, H, u_{g0}, v_{g0}, u_{gz}$, and v_{gz}. The resulting set of parameters $\{A(z), \phi(z), A, H, u_{g0}, v_{g0}, u_{gz}, v_{gz}\}$ therefore uniquely defines the idealized IO-coupled thermal wind balance that describes the formation and evolution of the LLJ for each 18-h case date. For further details, see [10].

2.2 Monotonic shear analogues

For comparison of turbine response to an LLJ inflow, we construct monotonically-sheared (MS) analogues at all time steps of the modeled LLJ case dates. The wind speed profile $V_{MS}(z)$ is given as a power law with altitude

$$V_{MS}(z) = V_{hub}\left(\frac{z}{z_{hub}}\right)^{\alpha} \tag{4}$$

where V_{hub} and z_{hub} are the turbine hub-height wind speed and altitude, respectively, and α is the power-law coefficient, fixed at 0.2 following the wind profile used in Design Load Cases (DLCs) for normal and selected extreme wind conditions [17]. The turbine hub height is fixed at $z_{hub} = 150$ m for the IEA 15 MW reference turbine used in this study. The final quantity V_{hub} is computed by matching the rotor-equivalent wind speed (with rotor diameter 240 m) for the MS case with the LLJ case.

The wind direction (and therefore the veer) of the MS case is exactly matched to the LLJ with respect to height. In contrast, similar studies that compare LLJ and MS profiles consider a MS inflow that has zero veer [8, 9]. Our loads analysis will therefore isolate the effects of positive and negative wind shear on turbine structural loading from the effects of veer in the wind profile.

2.3 Case studies

The analytically derived LLJ profiles presented in deJong, Quon, and Yellapantula and further considered in this work are presented alongside their MS-analogues for a few time snapshots in Figure 1. The MS analogues for all three cases have lower wind speeds below hub height and higher wind speeds above hub height in order to match the REWS of the LLJ profile. The 5 April 2020 case shows a clear jet nose that begins below hub height and gradually approaches hub height as the wind speeds increase, with wind speeds above cut-in at all times. This case also shows very strong local veer that changes sign across the turbine rotor, later stabilizing to a more constant veer. The 15 May 2020 case shows similar jet nose height behavior to 5 April, with the jet nose sitting above hub height later in the simulation. Wind speeds for this second case are on average significantly higher than the other two test cases, leading to the strongest REWS and also the strongest magnitude shears. The final 3 June 2020 test case shows a much weaker and broader jet with low wind speeds and a local maximum in wind speed that is sustained across most of the rotor layer. This broad LLJ results from a very stable boundary layer based on the fitting parameters of a 40 m scale height H and stability parameter $A = 0.4$ (see [10] and [18] for details) and therefore presents the largest veers among both LLJ and MS analogues.

As will be further described in section 3, the inflow conditions for turbine studies are defined as hourly snapshots from the 18 h trajectories of each LLJ and MS case study for a total of 54 snapshots for each wind-profile type. Properties of these snapshots are presented in aggregated in Figure 2 to indicate the distribution of test points with respect to wind speeds, veer, shear, and other key indicators. The distribution of wind speeds spans a characteristic range from near-zero and below cut-in to near the cutout wind speed of 25 m/s. For a single range of hub-height wind speeds, both the LLJ and MS cases sample two regimes of wind veer as illustrated in Figure 2 (top-left); for instance, at a hub-height wind speed of 20 m/s, the sampled conditions include both a near-zero veer as well as veer of approximately 0.008- deg/m. The LLJ cases similarly sample two regimes of mean shear (Figure 2, top-right) due to the evolution of the jet over its 18 h trajectory. This mean shear is always lower than for the MS cases due to the presence of a negative shear in the LLJ. The veer decreases with higher wind speeds, as expected for a less stable boundary layer, and the mean shear increases with wind speed. For the LLJ cases specifically, the magnitude of the negative shear is highest among cases which have moderate hub-height wind speeds (the 5 April 2020) test case, thus the importance of negative shear is not sampled as uniformly by these test cases. The distribution of the jet nose maximum wind speed and altitudes is clustered near and below the 150 m hub height and at moderate wind speeds between 10-25 m/s. This range is appropriate for studying the IEA 15MW turbine, but would present LLJ test cases with the maximum wind speed consistently

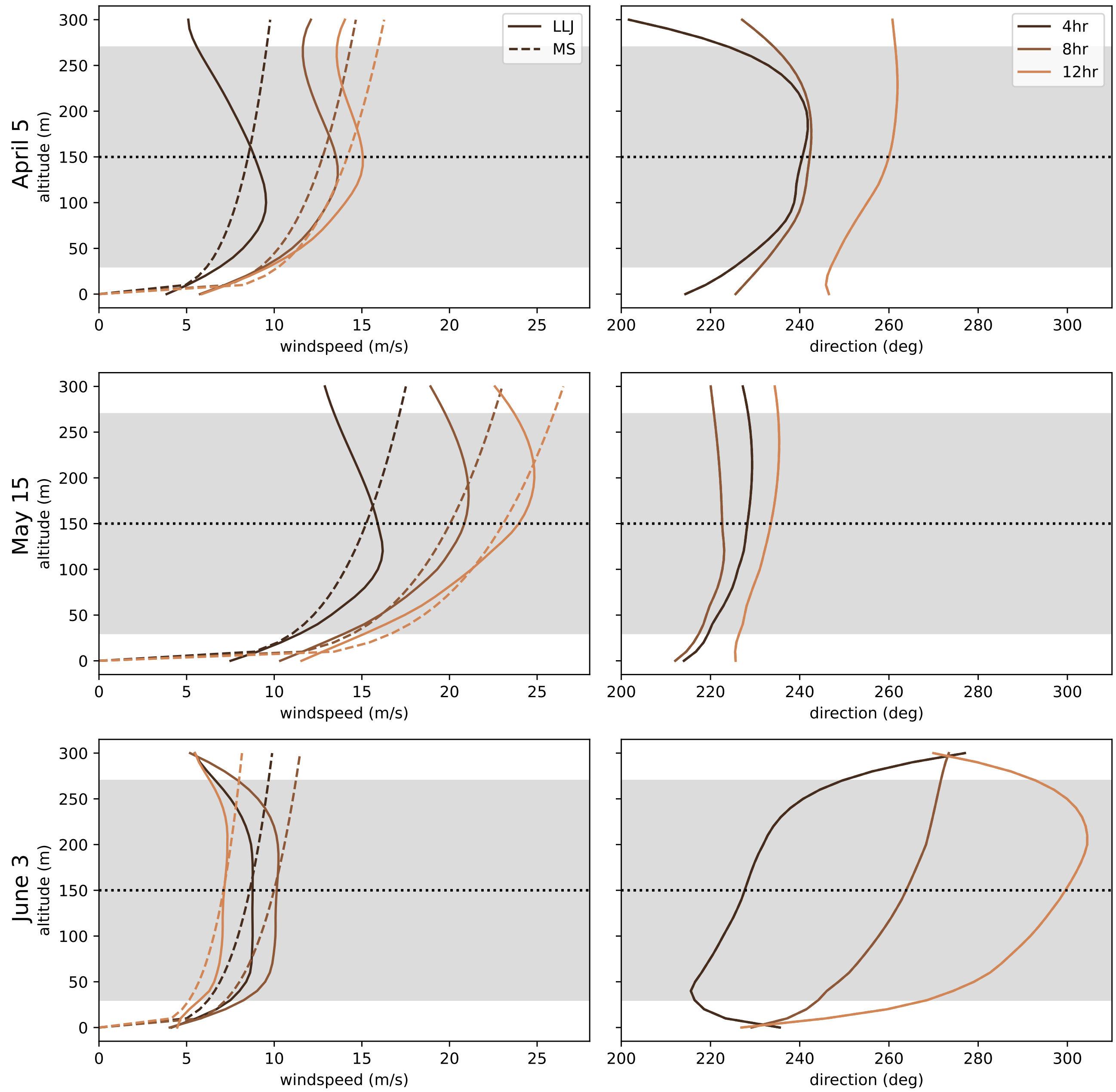

Figure 1: Snapshots at three different times (colors) of the wind speed (left) and wind direction (right) of the three idealized LLJ and monotonic wind cases: (top to bottom) 5 April 2020, 15 May 2020, 3 June 2020. Solid lines correspond to the LLJ and dashed lines correspond to the REWS and veer-matched monotonic shear case, MS. The dashed black line is the hub height of the IEA 15MW reference turbine, and the grey shaded area is the range of rotor swept altitude.

above or below the hub height in the case of different turbine studies, and thus does not systematically consider the influence of LLJ height.

3 Turbine Simulations in OpenFAST

OpenFAST provides a flexible multi-physics, multi-fidelity turbine simulation framework. For this investigation, we have focused on identifying trends in turbine dynamics rather than predicting turbine loads with the maximum accuracy afforded by the tool. The publicly available 15-MW Offshore Reference Wind Turbine model [16], developed through the International Energy Agency (IEA) Technology Collaboration Programme Wind Task 37, was simulated with OpenFAST v.3.5.0 [19].

We have considered the IEA 15-MW in a monopile configuration under still water conditions. Blade aerodynamic loads are calculated based on tabulated airfoil aerodynamics. Rotor inflow, discussed further in Section 3.1, includes turbulence superimposed by the TurbSim stochastic wind simulator in OpenFAST. Blade and tower structural dynamics are modeled by Euler-Bernoulli beam theory with assumed modes; substructure dynamics and platform motion have been neglected. Turbine control and electrical system dynamics are modeled using the Reference Open-Source Controller [20] and the tuned controller included with the IEA model.

3.1 Inflow conditions

We have assumed that the inflow is quasistationary, which enables us to evaluate hourly snapshots of the LLJ evolution rather than perform a continuous 18-h simulation. Inflow conditions for each snapshot were based on the time-averaged wind speed and direction over the following hour. We have also assumed that there is no yaw misalignment and, to facilitate the analysis, rotated the wind profile such that wind vector at hub height is aligned with the turbine inertial frame of reference. Each individual simulation was 12 minutes in length, with the initial 2 minutes excluded to neglect the effects of transients on the steady state analysis. Following the IEC 61400-1 standard [17], six 10-minute periods, corresponding to different turbulence field realizations, were evaluated for each snapshot.

Each of the three case studies from deJong, Quon, and Yellapantula were simulated, both under LLJ conditions and analogous monotonically sheared (“MS”) conditions. The MS conditions matched the LLJ conditions in rotor-equivalent wind speed (REWS) and wind direction profile, as described in section 2. These wind profiles were provided to TurbSim, which calculated turbulence boxes with IEC class C turbulence characteristics and de-

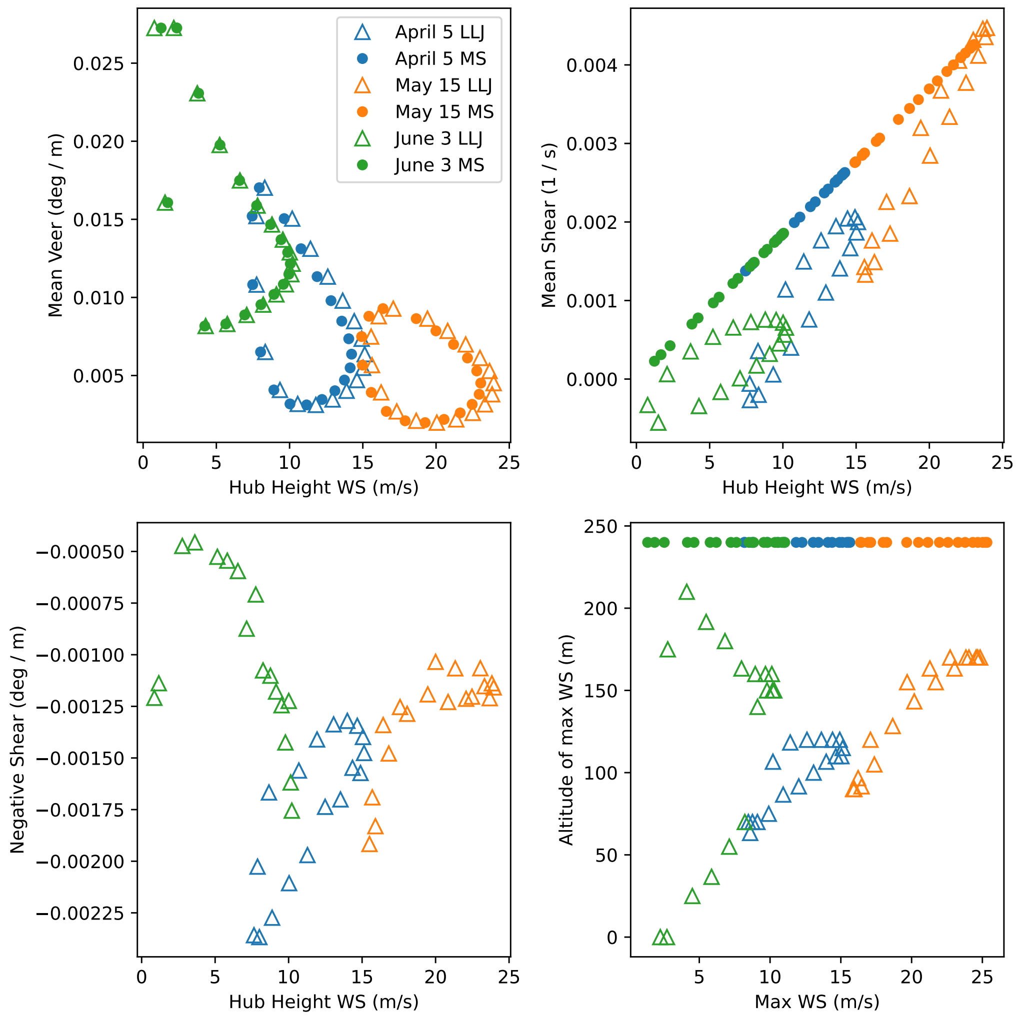

Figure 2: Distribution of hour inflow condition snapshots for LLJ cases (solid dots) and corresponding MS snapshots (triangles). Colors correspond to the model case date that each snapshot was generated from.

fault coherence parameters. The three case studies, two representative conditions per study, 18 hourly snapshots, and 6 turbulence realizations per snapshot total 648 ten-minute periods analyzed.

3.2 Output postprocessing

All simulations ran to completion with the exception of the May 15 case study between hour 9–16, when the wind speed exceeded the turbine cut-out speed (25 m/s). Statistics of each ten-minute analysis consider mean and standard deviation of the quantity over time (plotted as solid lines or individual points), as well as minimum and maximum of the quantity across each of the 6 turbulence realizations (which will be plotted as a shading). The distinction between these metrics of model spread are intended to indicate a difference in overall temporal fluctuations that contribute to structural fatigue (standard deviation), and the range of responses given six turbulence realizations.

4 Results

The preliminary results in this section consider the performance and structural impacts of the turbine in the context of the quantities summarized in Table 1. The hub-height inflow velocity is included for reference in Figures 3-5 and as the x-axis in Figures 5-7. Generated power is included in order to reference this study against other works which discuss the impacts of LLJs on turbine power production ([5, 9]), but these impacts are traced to different wake recovery characteristics that are not considered in this standalone single turbine study. Several structural parameters of the turbine are considered instead, including moments on the blade roots, low-speed shaft tip, tower-top, and tower-base. Other studies have found that properties of the LLJ had little impact on blade motions and loads [2, 9], but disagree on the impacts of loads applied to the hub center components (low-speed shaft and tower top). We begin by considering all of these output quantities in terms of their mean and temporal standard deviation as a proxy for fatigue loading on the turbine component. Later, we focus on a subset of these quantities that demonstrate the strongest differences between the LLJ and MS analogues to identify potential features of interest for turbine design under LLJ inflows.

4.1 Individual Case Studies

To gain an understanding of how turbine performance and loading may vary over the course of a typical LLJ event, which can persist for a few hours up to approximately a day, and identify quantities of interest, we begin by considering the collection of hourly snapshots from the 5 May 2020 case study. These inflow conditions

Abbreviation	Description (units)
HHWindVel	Hub Height inflow wind speed (m/s)
GenPwr	Generator power (kW)
RootMxb1	Edgewise blade moment (kNm)
RootMyb1	Flapwise blade moment (kNm)
LSSTipMys	Low-speed shaft tip pitching moment (kNm)
LSSTipMzs	Low-speed shaft tip yawing moment (kNm)
YawBrMyp	Pitching tower-top moment (kNm)
YawBrMzp	Yawing tower-top moment (kNm)
TwrBsMxt	Side-side tower base moment (kNm)
TwrBsMyt	Pitching tower-base moment (kNm)
TwrBsMzt	Yawing tower-base moment (kNm)

Table 1: Summary of the turbine quantities and their abbreviations.

(see Figures 1-2) display the highest wind speeds and shears for both the LLJ and MS, as well as characteristic magnitudes of the negative shear and location of the jet nose maximum. The 18 h trajectory corresponds to a full cycle of the inertial oscillation (Equation 1) about the stationary thermal wind balance, and thus demonstrates the full range of conditions for the LLJ given a constant geostrophic equilibrium profile. A comparison of the LLJ and MS inflow conditions from this perspective indicates which performance and loading quantities are inherent to the presence and evolution of the LLJ, versus those which are more indicative of local shear and veer regardless of the low-level windspeed maximum.

In Figure 3-4, we consider mean quantities as well as their standard deviations over time as a measure of the magnitude of fluctuations. As seen in Figure 3, the hub-height wind speeds increase over time to their maximum at around the 12th hour of the 18-h case study. Generator power for the LLJ and MS case are extremely close, reflecting the matched REWS, and fluctuations in the generator power are slightly higher for the LLJ than MS. This behavior contrasts findings that an LLJ reduces variance in power production [2, 9].

The mean flapwise blade-root moments are very similar between the two cases, with the LLJ also displaying smaller fluctuations in both flapwise and edgewise moments except for the flapwise moment at times corresponding with the strongest wind speeds near the cut-out speed of 25 m/s. The LLJ case displays consistently lower low-speed shaft tip moments, with negative moments occurring at lower wind speeds in contrast to the consistently positive moments in the MS case. The fluctuations in this LSSTip moments are, however, considerably higher for the LLJ case than the MS, indicating higher fluctuating loads on the shaft. This finding is consistent with similar studies that found an increase of up to 15% in the DEL on this component [9] when the wind resembled an LLJ profile.

The tower-top moments in Figure 4 tell a similar story to the low-speed shaft, with fluctuations (represented as the temporal standard deviation, in the right column) in both the pitching and yawing moments increasing substantially for an LLJ over the MS case. The mean yawing moments reflect a similar change in sign across the evolution of the LLJ, indicating impacts of the negative shear and jet nose height relative to the hub height. The mean tower-base moments generally mirror the tower-top moments, but the mean pitching moments at the tower base shows a broader range, from 60 MNm to 120 MNm across the evolution of both the LLJ and MS profiles, compared with the tower-top pitching moment range magnitudes of 45 MNm to 65 MNm.

Next, we consider all three case studies, focusing on a subset of the structural quantities which showed the most distinctive differences between the LLJ and MS analogues. In Figure 5, each subplot shows the trajectory of the mean quantity and shading corresponding to one standard deviation above and below the mean. To aid in the analysis, we further characterize each case study according to its jet characteristics as seen in Figure 1, with 3 June 2020 displaying a broad jet, 5 April 2020 showing a narrow jet near hub height, and 15 May 2020 having a narrow jet that rises above hub height. Across all three test cases, we see in Figure 5 that both the edgewise and flapwise blade moments are extremely similar between the LLJ and MS cases, with similar magnitudes of the temporal fluctuations as well. The tower-top quantities in the second row, however, show important differences. The pitching moments are of consistently larger magnitudes for the LLJ than for the MS, especially during periods of the jets where the jet nose is below or near the hub height. This difference indicates consistently larger magnitude motions at the tower top under an LLJ, which may not be accounted for under typical MS design studies. The yawing tower top moment and pitching low-speed shaft moments also have opposite sign in the LLJ case from the MS case at times when there is a deviation, but the magnitudes of temporal fluctuation are similar. Finally, the tower-base fore-aft is similar between LLJ and MS in all three instances, with differences appearing mainly in the 15 May 2020 case study, which contains the strongest wind speeds and shears but a decrease in the tower-base moments relative to the MS case.

4.2 Aggregated Structural Impacts

A cross-examination of figures 5 and 1 reveals that turbine moments are correlated with the hub-height wind speeds as expected. Thus in Figure 6, we ignore the trajectory of the LLJ and MS cases over their 18-h evolution and instead consider each 10 min simulation independently to elucidate key operating differences in the presence

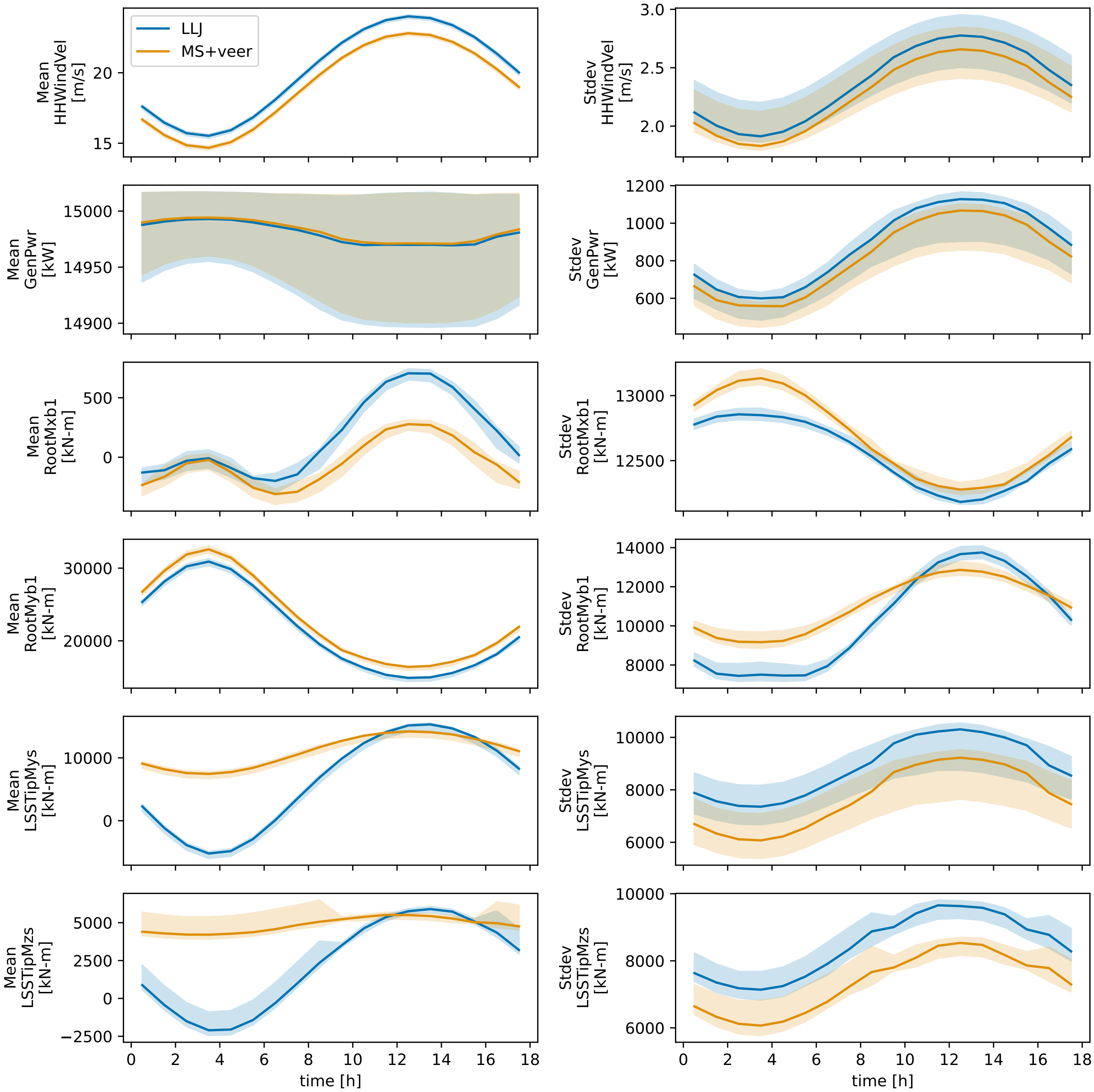

Figure 3: Turbine quantity means (left) and standard deviations (right) as a function of time for the 15 May 2020 case, including the LLJ and corresponding veered MS profiles. (Top to bottom) Hub height inflow wind velocity, generator inflow power, flapwise blade moment, edgewise blade moment, low-speed shaft tip (LSST) bending moments in-plane and out-of-plane. Statistical convergence was not reached in some turbulence realizations for the LSST quantities, hence the reduced shading between 10 and 15 hrs.

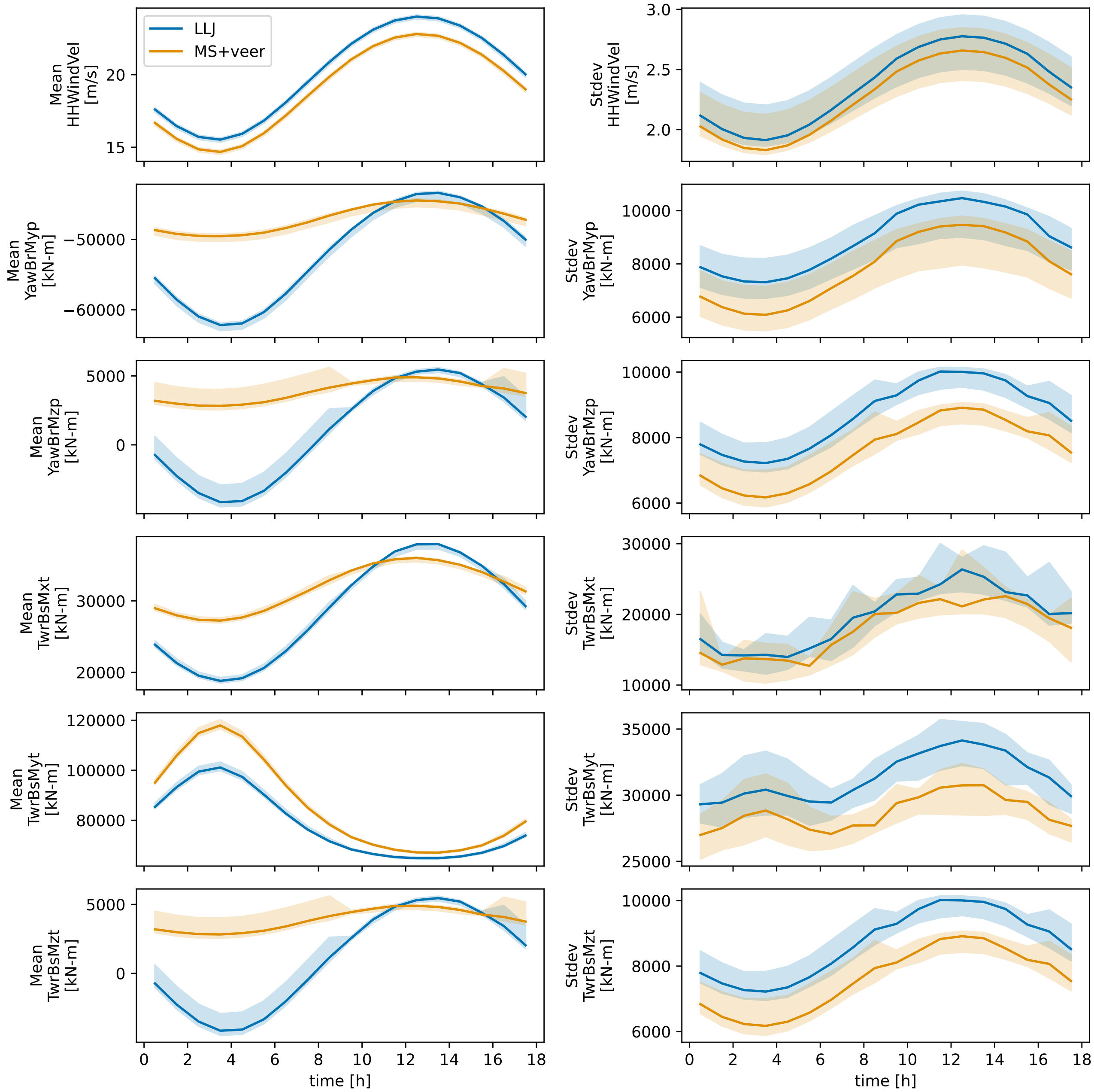

Figure 4: Turbine quantity means (left) and standard deviations (right) as a function of time for the 15 May 2020 case, including the LLJ and corresponding veered MS profiles. (Top to bottom) Hub height inflow wind velocity, tower-top yaw-bearing roll moment, tower-top yaw-bearing pitch moment, and tower base roll, pitching, and yaw moments. Statistical convergence was not reached in some turbulence realizations for the tower top and base quantities, hence the reduced shading between 10 and 15 hrs.

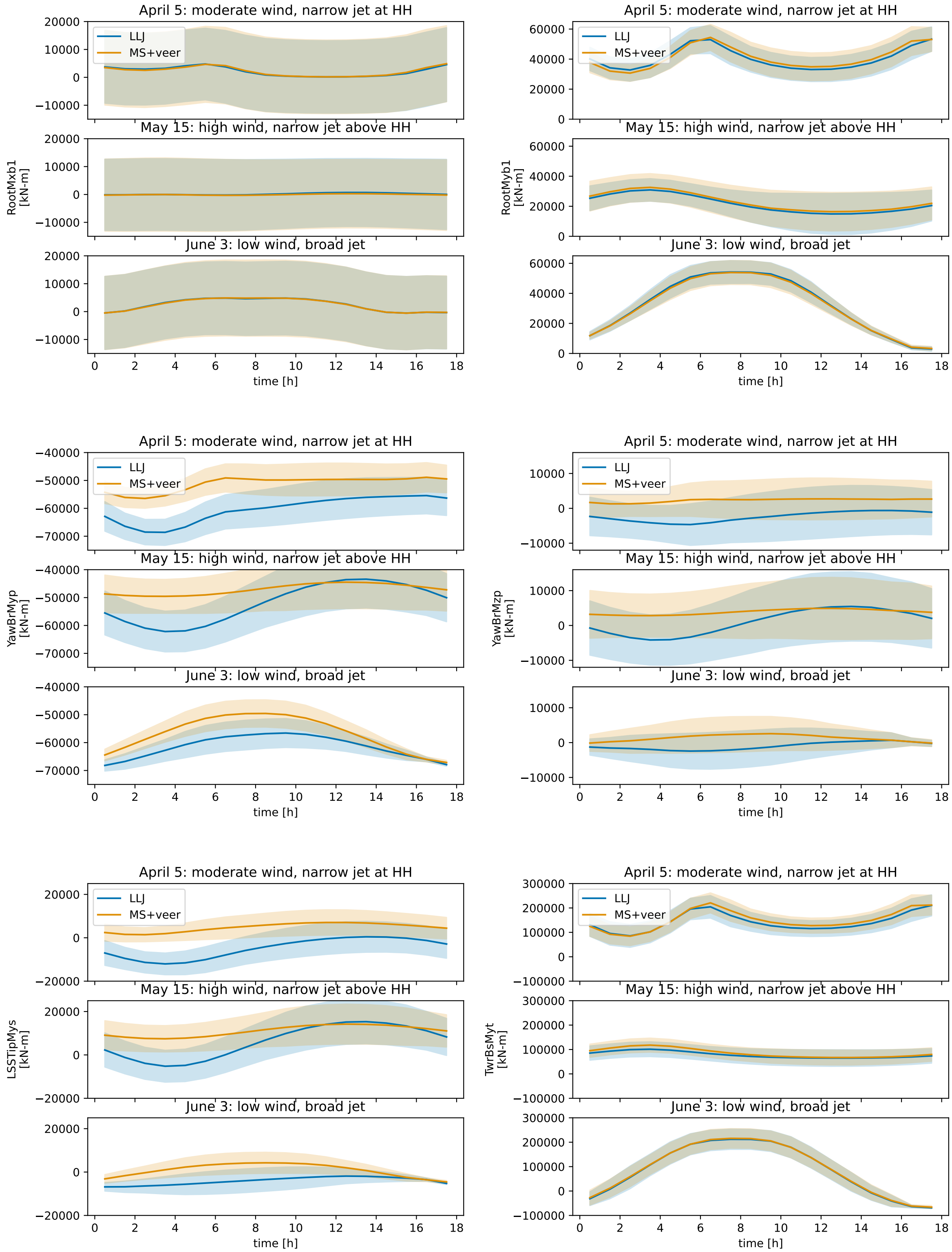

Figure 5: Trajectory of core turbine quantities for each LLJ and MS cases. Each quantity is plotted as the temporal mean (solid line) plus or minus the temporal standard deviation (shading), with these statistics referring to the median from the six turbulence realizations.

of a jet. The LLJ and MS cases collapse onto a single line that correlates the mean flapwise blade moment with this hub-height wind speed, with the maximum flapping occurring when thrust is maximized at wind speeds near 10 m/s. Fluctuations in this flapping, measured by the temporal standard deviation, show stronger variation between turbulence realizations, with a bias of larger fluctuations in the LLJ than the MS cases at low wind speeds and smaller fluctuations at high wind speeds. This result indicates the potential for reduced blade fatigue due to flapwise motions during strong and sustained LLJ events such as the 15 May 2020 case study.

Next, we note an interesting bifurcation in the pattern of mean tower-top and low-speed shaft moments. While the pitching and yawing moments both increase nearly monotonically with wind speed for the MS cases, the LLJ simulations show a cyclic behavior with respect to hub-height wind speed. This cyclic behavior is indicative of the different positions of the jet wind maximum with respect to the turbine hub as well as the different magnitudes of shear and veer associated with a single hub-height wind speed, as seen in Figure 2. It further implies that these quantities cannot be easily predicted by an average or hub height inflow wind speed in the case of an LLJ, and it indicates a wider potential operating range in the presence of an LLJ, which may be important in future turbine design. The standard deviation of all three quantities generally increases with hub-height wind speed, indicating stronger pitching and yawing motions under stronger wind speeds. These fluctuations are somewhat higher for LLJ than for MS cases, but the spread across turbulence realizations largely obscures this difference, indicating that these fluctuating quantities are as strong a function of turbulent inflow as they are of the LLJ or MS condition.

Revisiting the cyclic behavior of the tower-top quantities with respect to hub-height wind speed, Figure 7 depicts the envelope of operating conditions encountered for the four key turbine quantities as a function of this inflow wind speed. As noted in the previous paragraph, there is no discernible difference in the operating range of flapwise blade moments between the LLJ and MS case. However, the pitching moments of both tower-top components indicate a significantly wider operating envelope, in particular at more negative (higher magnitude) moments across all inflow wind speeds. The tower top yawing moment shows similar behavior, with the LLJ inflow conditions spanning nearly the same range of conditions in the positive moment direction, but encountering larger magnitude negative moments. This difference in operating envelope stems from the presence of a negative shear in the LLJ inflow conditions, and may have design implications for the turbine tower if these negative moments exceed those in extreme negative wind shear cases (DLC 1.5).

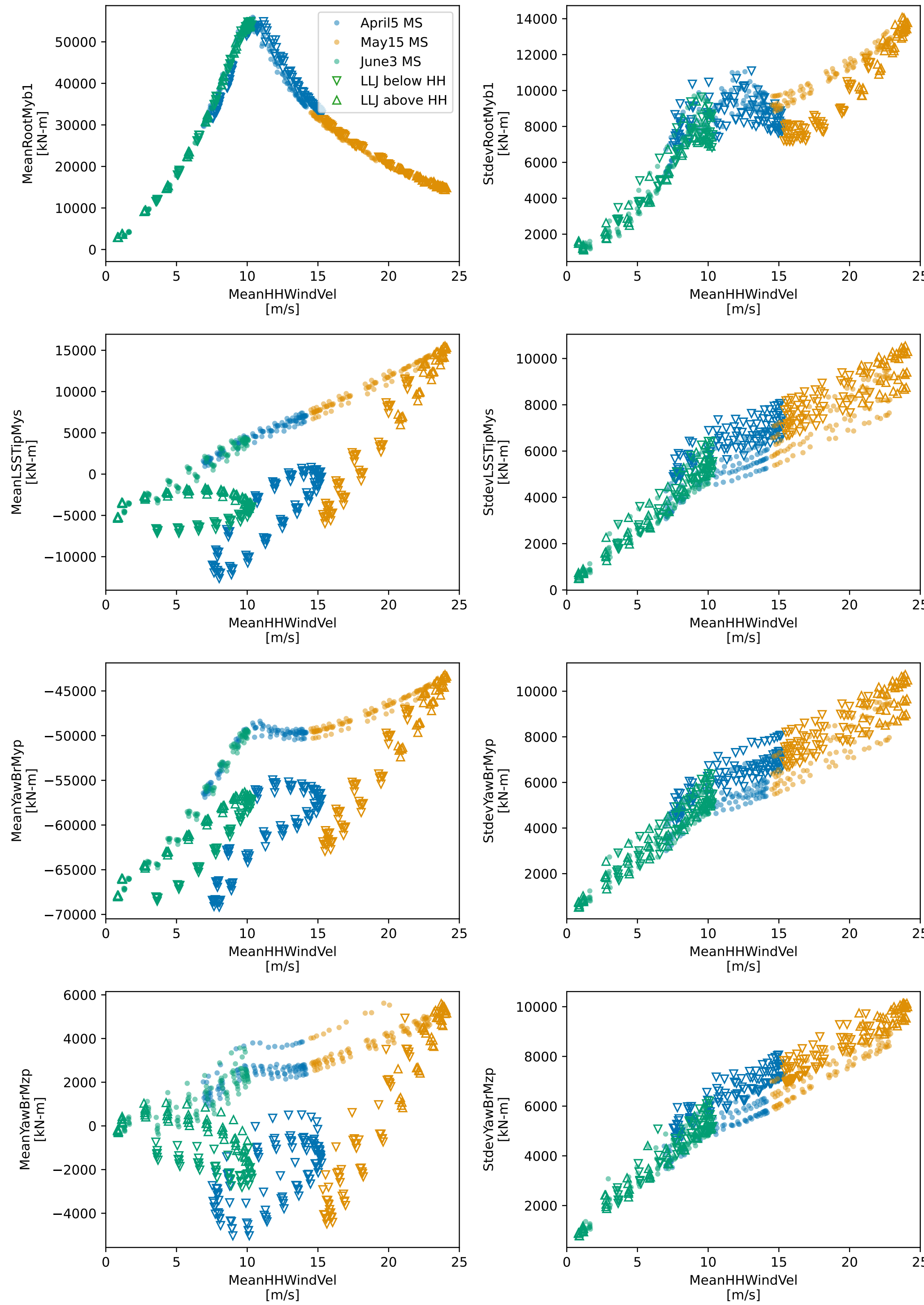

Figure 6: Mean (left) and standard deviation (right) of turbine quantities for all turbulence realizations, plotted for each case day (color) and LLJ or MS (symbol) as a function of the hub-height inflow wind velocity. We further distinguish LLJ instances where the LLJ maximum velocity occurs below or above hub height (downward and upward triangles, respectively). (Top to bottom) Blade flapwise moment, LSST in-plane bending, and tower-top pitching and yawing moments.

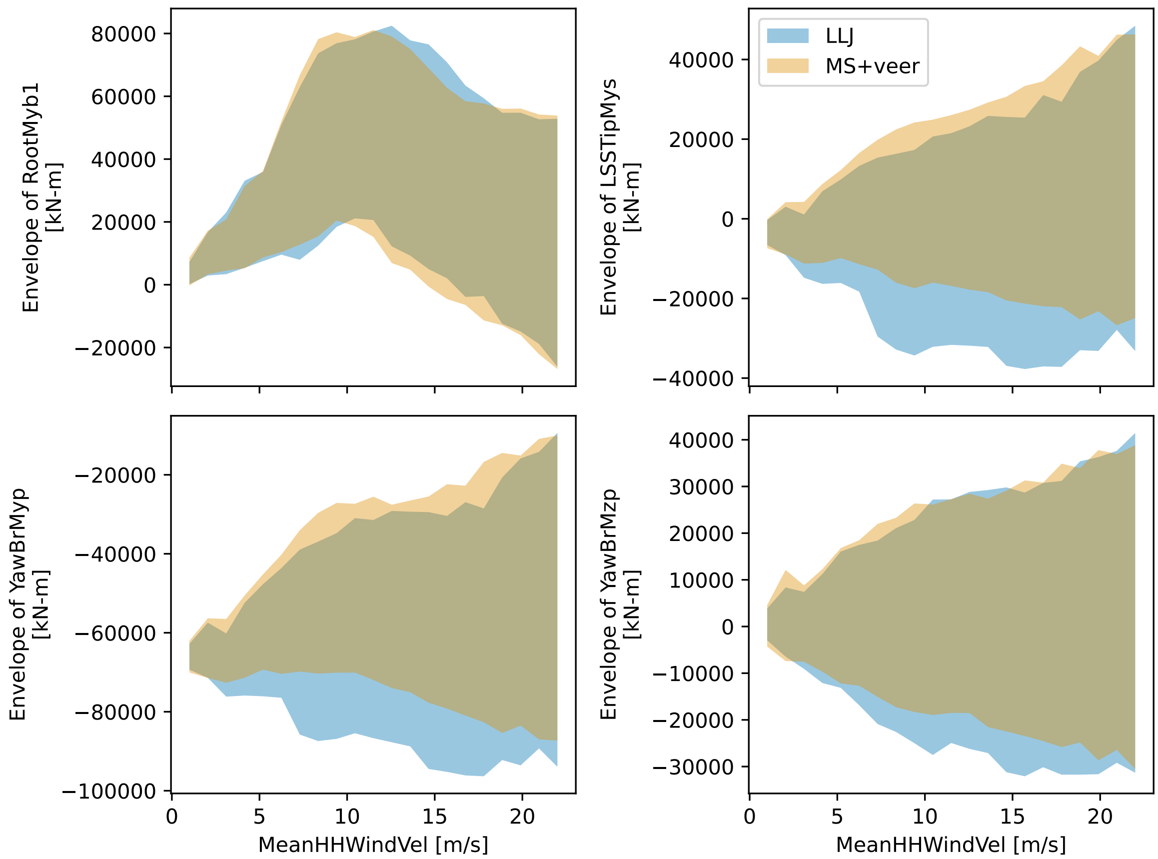

Figure 7: Operating envelope of selected turbine quantities for the LLJ and MS settings, plotted as the range from the minimum to maximum across the three case dates and turbulence realizations.

5 Conclusions

This work presents an analysis of the structural impacts of low-level jets on turbine components based on an analytical representation of an evolving jet profile. We describe a set of prognostic equations for the LLJ wind components as a function of height that results from an inertial rotation of the wind vector about a geostrophic balance [10]. For three case studies based on observed LLJs in the NY Bight, we note that these analytical models generate inflow conditions that span a range of wind speeds, shear, veer, and LLJ altitude conditions of potential interest to offshore turbine design. These equations therefore present a streamlined model with a simple set of tunable parameters that can be adjusted to study a range of realistic LLJ inflow conditions, making them suitable for future integration in DLCs for offshore turbine design.

Our preliminary study of turbine performance under these LLJ and MS analogue inflows investigates differences in the generated power and structural loads of the IEA 15-MW offshore reference turbine under these conditions with class C turbulence. Similar to previous studies [2, 7, 9], we find minimal impacts of the LLJ on the generated power for this single turbine given the same REWS. Mean and fluctuating moments on the turbine blades likewise show similar behavior for the LLJ and MS analogue, and these moments reduce to a single relationship with the hub height inflow wind speed. However, tower-top moments, including pitching and yawing moments on the low-speed shaft and the yaw-bearing, tell a different story. We find that the LLJ induces larger magnitude moments on the tower top as well as somewhat larger fluctuating loads, leading to an overall larger range of potential operating conditions under LLJ inflow than for the same inflow wind speeds in MS conditions. These LLJ loads are not necessarily predicted by an average or hub height inflow wind speed. Additional work is necessary to compare the turbine impacts of these idealized LLJ inflows with existing IEC standards for negative shear, such as DLC 1.5 [17]. However, with increasing interest and development of offshore wind energy in the U.S. Mid-Atlantic, this finding indicates a need to detect and control for increased fatigue on these yaw-bearing components when LLJs are present.

Data Availability Scripts to set up, run, and postprocess the OpenFAST simulations detailed herein may be downloaded from [21].

References

[1] Xuyao Zhang, Congxin Yang, and Shoutu Li. "Influence of the Heights of Low-Level Jets on Power and Aerodynamic Loads of a Horizontal Axis Wind Turbine Rotor". en. In: *Atmosphere* 10.3 (Mar. 2019). Number: 3 Publisher: Multidisciplinary Digital Publishing Institute, p. 132. DOI: 10.3390/atmos10030132. URL: https://www.mdpi.com/2073-4433/10/3/132 (visited on 09/17/2021).

[2] Walter Gutierrez et al. "Impacts of the low-level jet's negative wind shear on the wind turbine". English. In: *Wind Energy Science* 2.2 (Nov. 2017). Publisher: Copernicus GmbH, pp. 533–545. ISSN: 2366-7443. DOI: 10.5194/wes-2-533-2017. URL: https://wes.copernicus.org/articles/2/533/2017/ (visited on 08/23/2021).

[3] David J. Stensrud. "Importance of Low-Level Jets to Climate: A Review". EN. In: *Journal of Climate* 9.8 (Aug. 1996). Publisher: American Meteorological Society Section: Journal of Climate, pp. 1698–1711. ISSN: 0894-8755, 1520-0442. DOI: 10.1175/1520-0442(1996)009<1698:IOLLJT>2.0.CO;2. URL: https://journals.ametsoc.org/view/journals/clim/9/8/1520-0442_1996_009_1698_iolljt_2_0_co_2.xml (visited on 01/10/2022).

[4] Jeanie A. Aird et al. "Occurrence of Low-Level Jets over the Eastern U.S. Coastal Zone at Heights Relevant to Wind Energy". en. In: *Energies* 15.2 (Jan. 2022). Number: 2 Publisher: Multidisciplinary Digital Publishing Institute, p. 445. ISSN: 1996-1073. DOI: 10.3390/en15020445. URL: https://www.mdpi.com/1996-1073/15/2/445 (visited on 02/23/2023).

[5] W. Gutierrez et al. "Structural impact assessment of low level jets over wind turbines". In: *Journal of Renewable and Sustainable Energy* 8.2 (Mar. 2016). Publisher: American Institute of Physics, p. 023308. DOI: 10.1063/1.4945359. URL: https://aip.scitation.org/doi/10.1063/1.4945359 (visited on 08/23/2021).

[6] Walter Gutierrez et al. "The structural response of a wind turbine under operating conditions with a low-level jet". en. In: *Renewable and Sustainable Energy Reviews* 108 (July 2019), pp. 380–391. ISSN: 1364-0321. DOI: 10.1016/j.rser.2019.03.058. URL: https://www.sciencedirect.com/science/article/pii/S1364032119301984 (visited on 08/23/2021).

[7] Ali Doosttalab et al. "Interaction of low-level jets with wind turbines: On the basic mechanisms for enhanced performance". In: *Journal of Renewable and Sustainable Energy* 12.5 (Sept. 2020). Publisher: American Institute of Physics, p. 053301. DOI: 10.1063/5.0017230. URL: https://aip.scitation.org/doi/10.1063/5.0017230 (visited on 12/08/2021).

[8] Srinidhi N. Gadde and Richard J. A. M. Stevens. "Effect of low-level jet height on wind farm performance". In: *Journal of Renewable and Sustainable Energy* 13 (2020). DOI: `https://doi.org/10.1063/5.0026232`. URL: `https://aip.scitation.org/doi/10.1063/5.0026232` (visited on 07/09/2021).

[9] Tanmoy Chatterjee et al. "Wind farm response to mesoscale-driven coastal low level jets: a multiscale large eddy simulation study". en. In: *Journal of Physics: Conference Series* 2265.2 (May 2022). Publisher: IOP Publishing, p. 022004. ISSN: 1742-6596. DOI: `10.1088/1742-6596/2265/2/022004`. URL: `https://dx.doi.org/10.1088/1742-6596/2265/2/022004` (visited on 05/18/2023).

[10] Emily deJong, Eliot Quon, and Shashank Yellapantula. "Mechanisms of Low-Level Jet Formation in the U.S. Mid-Atlantic Offshore". In: *Submitted to Journal of Atmospheric Sciences* in review (2023). URL: `https://edejong-caltech.github.io/files/2023-lljs.pdf`.

[11] NYSERDA. *Resource Panorama Public Data*. URL: `https://oswbuoysny.resourcepanorama.dnvgl.com/download/f67d14ad-07ab-4652-16d2-08d71f257da1` (visited on 08/23/2021).

[12] Alfred K. Blackadar. "Boundary Layer Wind Maxima and Their Significance for the Growth of Nocturnal Inversions". en. In: *Bulletin of the American Meteorological Society* 38.5 (May 1957). ISBN: 9781520047737 Publisher: American Meteorological Society Section: Bulletin of the American Meteorological Society, pp. 283–290. ISSN: 0003-0007, 1520-0477. DOI: `10.1175/1520-0477-38.5.283`. URL: `https://journals.ametsoc.org/view/journals/bams/38/5/1520-0477-38_5_283.xml` (visited on 12/23/2020).

[13] B. J. H. Van de Wiel et al. "A Conceptual View on Inertial Oscillations and Nocturnal Low-Level Jets". EN. In: *Journal of Atmospheric Sciences* 67.8 (Aug. 2010). Publisher: American Meteorological Society Section: Journal of Atmospheric Sciences, pp. 2679–2689. ISSN: 0022-4928, 1520-0469. DOI: `10.1175/2010JAS3289.1`. URL: `https://journals.ametsoc.org/view/journals/atsc/67/8/2010jas3289.1.xml` (visited on 12/23/2020).

[14] Thomas R. Parish. "Forcing of the Summertime Low-Level Jet along the California Coast". EN. In: *Journal of Applied Meteorology and Climatology* 39.12 (Dec. 2000). Publisher: American Meteorological Society Section: Journal of Applied Meteorology and Climatology, pp. 2421–2433. ISSN: 1520-0450, 0894-8763. DOI: `10.1175/1520-0450(2000)039<2421:FOTSLL>2.0.CO;2`. URL: `https://journals.ametsoc.org/view/journals/apme/39/12/1520-0450_2000_039_2421_fotsll_2.0.co_2.xml` (visited on 06/14/2021).

[15] Vern Ostdiek and William Blumen. “A Dynamic Trio: Inertial Oscillation, Deformation Frontogenesis, and the Ekman–Taylor Boundary Layer”. EN. In: *Journal of the Atmospheric Sciences* 54.11 (June 1997). Publisher: American Meteorological Society Section: Journal of the Atmospheric Sciences, pp. 1490–1502. ISSN: 0022-4928, 1520-0469. DOI: `10.1175/1520-0469(1997)054<1490:ADTIOD>2.0.CO;2`. URL: `https://journals.ametsoc.org/view/journals/atsc/54/11/1520-0469_1997_054_1490_adtiod_2.0.co_2.xml` (visited on 08/19/2021).

[16] Evan Gaertner et al. *Definition of the IEA 15-Megawatt Offshore Reference Wind*. Tech. rep. TP-5000-75698. Golden, CO: National Renewable Energy Lab, 2020. URL: `https://www.nrel.gov/docs/fy20osti/75698.pdf` (visited on 08/23/2021).

[17] International Electrotechnical Commission. *Wind Energy Generation Systems - Part 1: Design Requirements*. Tech. rep. IEC 61400-1, Edition 4.0. Geneva, Switzerland: International Electrotechnical Commission, Feb. 2019.

[18] Vern Ostdiek and William Blumen. “Deformation Frontogenesis: Observation and Theory”. EN. In: *Journal of the Atmospheric Sciences* 52.9 (May 1995). Publisher: American Meteorological Society Section: Journal of the Atmospheric Sciences, pp. 1487–1500. ISSN: 0022-4928, 1520-0469. DOI: `10.1175/1520-0469(1995)052<1487:DFOAT>2.0.CO;2`. URL: `https://journals.ametsoc.org/view/journals/atsc/52/9/1520-0469_1995_052_1487_dfoat_2_0_co_2.xml` (visited on 01/26/2023).

[19] Bonnie Jonkman et al. *OpenFAST/Openfast: V3.5.0*. Zenodo. May 2023. DOI: `10.5281/zenodo.7942867`.

[20] Nikhar J. Abbas et al. *NREL/ROSCO: Version 2.8.0*. Zenodo. Apr. 2023. DOI: `10.5281/zenodo.7818525`.

[21] Eliot Quon. *Ewquon/Openfast-LLJ-study: NAWEA/WindTech 2023*. Zenodo. Oct. 2023. DOI: `10.5281/zenodo.10049486`.